Review Article

Tools for cardiovascular magnetic resonance imaging

Ramkumar Krishnamurthy, Benjamin Cheong, Raja Muthupillai

Department of Diagnostic and Interventional Radiology, CHI St. Luke's Health, Texas Medical Center, Houston, Texas 77030, USA
Correspondence to: Raja Muthupillai. Department of Diagnostic and Interventional Radiology, St. Luke's Hospital, Texas Medical Center, 6720 Bertner Avenue, Houston, Texas 77030, USA. Email: rmuthupillai@stlukeshealth.org.

Abstract: In less than fifteen years, as a non-invasive imaging option, cardiovascular MR has grown from a being a mere curiosity to becoming a widely used clinical tool for evaluating cardiovascular disease. Cardiovascular magnetic resonance imaging (CMRI) is now routinely used to study myocardial structure, cardiac function, macro vascular blood flow, myocardial perfusion, and myocardial viability. For someone entering the field of cardiac MR, this rapid pace of development in the field of CMRI might make it difficult to identify a cohesive starting point. In this brief review, we have attempted to summarize the key cardiovascular imaging techniques that have found widespread clinical acceptance. In particular, we describe the essential cardiac and respiratory gating techniques that form the backbone of all cardiovascular imaging methods. It is followed by four sections that discuss: (I) the gradient echo techniques that are used to assess ventricular function; (II) black-blood turbo spin echo (SE) methods used for morphologic assessment of the heart; (III) phase-contrast based techniques for the assessment of blood flow; and (IV) CMR methods for the assessment of myocardial ischemia and viability. In each section, we briefly summarize technical considerations relevant to the clinical use of these techniques, followed by practical information for its clinical implementation. In each of those four areas, CMRI is considered either as the benchmark imaging modality against which the diagnostic performance of other imaging modalities are compared against, or provides a complementary capability to existing imaging techniques. We have deliberately avoided including cutting-edge CMR imaging techniques practiced at few academic centers, and restricted our discussion to methods that are widely used and are likely to be available in a clinical setting. Our hope is that this review would propel an interested reader toward more comprehensive reviews in the literature.

Keywords: Cardiovascular magnetic resonance imaging (CMRI); cardiac functional imaging; myocardial ischemia imaging; myocardial structural imaging; myocardial viability imaging

Submitted Nov 04, 2013. Accepted for publication Feb 08, 2014.
doi: 10.3978/j.issn.2223-3652.2014.03.06
View this article at: http://www.thecdt.org/article/view/3639/4519

Clinical management of patients with heart disease is facilitated with accurate information regarding the underlying pathology, which may manifest as alterations in myocardial structure, function, macro and micro-vascular blood flow, viability, and metabolism. Non-invasive diagnostic imaging modalities such as echocardiography, radio-tracer based nuclear studies, X-ray computed tomography, and magnetic resonance imaging (MRI) are routinely used to help the clinician to evaluate the underlying pathologic changes. As a non-invasive imaging modality, MRI provides a number of mechanisms that can be effectively manipulated to generate different types of contrast. For example, MR images with different contrast weightings based on tissue magnetic relaxation parameters such as spin-lattice relaxation (T_1), spin-spin relaxation (T_2) can provide varied soft-tissue contrast between normal and pathologic states of tissue and can be used to assess tissue *structure*. In the last decade MR based methods have advanced sufficiently to provide cardiac gated tomographic images of the moving heart with exquisite spatial (1-2 mm in-plane resolution), temporal (50 ms or better) and contrast resolutions (1-3). Such advances have enabled routine assessment of *cardiac function and blood flow*. In conjunction with the administration of MR contrast agents, MR methods have been adapted to yield information

about myocardial *viability* and myocardial *perfusion* (4-8). While not yet a routinely used clinical tool, MR spectroscopy (MRS) is a research tool widely used to study myocardial metabolism (9,10).

The limitations of MR are: (I) it is not suitable for imaging extremely large patients, or patients with significant issues of claustrophobia; (II) it is also not suitable for patients with non-MR compatible implants, and Gadolinium-based MR contrast administration is often restricted to patients with good renal artery function; and (III) the scan time efficiency of MR is intrinsically lower than X-ray computed tomography, or echo ultrasound.

Nevertheless, the promise of comprehensive evaluation of cardiovascular disease is one of the attractive features of cardiac MR. This multi-faceted ability of cardiac MR often makes it the arbitrating imaging modality in patients with equivocal test results obtained via other imaging evaluations. Recent results from the EuroCMR registry (with over 27,000 patients) suggest that cardiovascular MR imaging (CMRI) provides information that can impact patient management in over 60% of the subjects who underwent CMRI (11).

The organization of this article is as follows. We first provide the technical requirements of cardiovascular imaging in terms of respiratory and cardiac gating. In subsequent sections, we sequentially describe the MR imaging techniques commonly used to measure myocardial mechanical function, myocardial structure, micro and macrovascular blood flow, and myocardial ischemia and viability. In each section, we attempt to provide a brief overview of the technical principles involved and their clinical applications. There are exhaustive reviews in the literature about these techniques for each of the methods described here, and the scope of this review is restricted to provide a brief overview of the clinically used cardiovascular MR imaging techniques.

Technical preliminaries for CMRI

A brief outline of MR imaging experiment

For a detailed description about the origin of the MR signal and the spatial encoding process, the reader is referred elsewhere (12). In brief, hydrogen nuclei, the source of MR signal, is the most abundant atom in the human body, primarily as a constituent of water and fat. While the precise formulation of the MR signal formation requires a quantum mechanical description, three essential steps through which a measurable proton magnetization is created can be described using a simple classical model as described in *Figure 1*. Please refer to the caption for details.

The transverse magnetization precessing at Larmor frequency induces an electric signal in a properly oriented receiver coil. By well-defined spatial modulation of the strength of the magnetic field, the received MR signal can be spatially encoded for the purposes of image formation. The experimental parameters such as the flip angle, the time between the application of successive RF pulses to create transverse magnetization (repetition time or TR), and the time at which the signal is measured after the excitation (TE) can be freely altered in an MR experiment to generate images that highlight a specific type of soft-tissue contrast, e.g., T_1 weighted, T_2 weighted, proton density (PD) weighted etc.

CMRI—addressing the effects of motion

Because cardiac pulsation, respiration, and blood flow (13) can degrade MR image quality it is necessary to take additional measures to combat the deleterious effects of such motion. Some of the commonly used approaches to combat the motion-induced artifacts in CMRI are briefly summarized below.

Cardiac motion

Cardiac gating is essential to minimize detrimental effect on image quality due to cardiac motion during data acquisition. In its simplest implementation, commonly referred to as *prospective* gating, MR acquisition occurs at a pre-defined portion of the cardiac cycle (e.g., in diastole) after the MR scanner detects the upslope of an 'R' wave in the ECG signal. All phase encoding steps necessary for the image formation are acquired at the same temporal location of the ECG over one or more RR intervals.

Single phase cardiac imaging

In single phase cardiac acquisitions, the MR scanner commences data acquisition only after an user-defined period has elapsed from the machine recognition of the R wave (trigger delay). Data acquisition window is typically limited to few tens of milliseconds per RR interval to minimize cardiac motion, and this process is repeated over multiple RR intervals, until all phase encoding steps necessary to form the image are collected. Attempts to improve the data acquisition efficiency by either prolonging the acquisition window or acquiring multiple slices per RR interval can result in increased sensitivity to motion artifacts or acquisition of

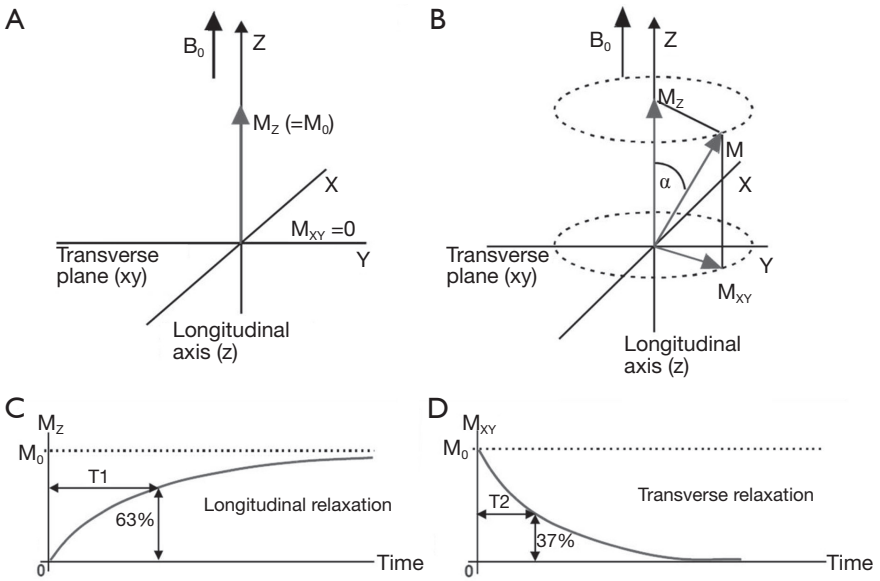

Figure 1 (A) An externally applied strong magnetic field (commonly referred to as the B_0 field), creates a slight excess of protons aligned parallel to B_0 than against it. This small excess of protons provides the source of measurable MR signal or M_0. M_0 precesses about B_0 with a frequency that is proportional to B_0. By convention, the axis along which B_0 is applied is referred to as the '*Z*' axis, or longitudinal axis, and the plane perpendicular to the longitudinal axis is the '*XY*' plane or transverse plane; (B) RF excitation: application of RF energy at the precessional frequency tips M_0 away from the Z axis, creating transverse magnetization (M_{XY}). The amount of tilt away from the Z axis or the *flip angle*, is proportional to the strength, shape and duration of the RF pulse. An RF pulse that completely rotates M_Z into the transverse plane is called a 90° RF pulse; (C,D) relaxation: after the termination of the RF pulse the magnetization "relaxes" back toward M_0 emitting the absorbed RF energy through interaction with the surrounding lattice (spin-lattice or longitudinal relaxation), and through interaction with neighboring protons (spin-spin or transverse relaxation). The rate of longitudinal relaxation is characterized by a time constant (T_1)-defined as the time it takes for spins to reach 63% of M_0 following the application of a 90º RF excitation. The rate at which spins lose their phase coherence due to spin-spin interactions in the transverse plane is characterized by another time constant (T_2)-the time it takes for the amplitude of the transverse magnetization to decay to 37% of the M_0 after the application of a 90º excitation. It should be emphasized that these two forms of relaxation are *independent* of each other and occur simultaneously.

some data during systole when cardiac motion is significant. In this context, for spin echo (SE) imaging methods (discussed below), note that TR is essentially determined by the heart rate. For example, at a heart rate of 60 bpm the RR interval, TR is 1,000 ms. At lower heart rates, TR is further prolonged making it difficult to obtain good T_1 weighted SE contrast.

Multi-phase or cine cardiac imaging

In *prospective gating*, following the detection of the R wave, a subset of phase encoding steps necessary for image formation is repeatedly acquired, for a pre-defined duration and the acquisition is discontinued until the next R wave is detected. Phase encoding steps are progressively incremented following the detection of each R wave until all necessary phase encoding steps to make an image are acquired. These images are then presented in the order in which the data were acquired, i.e., with increasing delays from the R wave, to create a cine loop of cardiac motion. The key disadvantage of prospective gating is the 'dead time' between RR intervals, when the scanner is waiting for the next RR interval. This can result in jumpy movie loops (e.g., missing the atrial contraction at end-diastole), or more seriously, result in underestimation of aortic regurgitation that may occur in late diastole.

In contrast, with *retrospective gating*, a single phase encoding step or a sub-set of phase encoding steps required to form an image is repeatedly acquired throughout the RR interval while simultaneously recording the temporal information about when data sampling occurred with respect to the R wave (14). At the conclusion of one cardiac cycle, the phase encoding step(s) are incremented, and acquisition proceeds until all necessary data is collected. After the completion of the data acquisition,

with the knowledge of the temporal location of phase encoding steps, images can be reconstructed at any user-prescribed temporal resolution. Most modern scanners use retrospective cardiac gating for multi-phase cine imaging, in conjunction with arrhythmia rejection to discard data from ectopic or arrhythmic beats.

Respiratory motion

Breathholding

The expansion and contraction of the thoraco-abdominal cavity with respiration displaces the heart substantially (15). While breathholding is an effective strategy to minimize respiratory motion induced artifacts, most adult cardiac patients can reproducibly hold their breath only for about 12-18 heart beats (13). This duration puts an upper limit on the attainable coverage/resolution for most clinical imaging under suspended respiration. To breach this ceiling, several forms of respiratory gating have been developed to allow imaging during free breathing, and these techniques vary considerably in their sophistication. The commonly used respiratory gating methods include some variation of averaging, respiratory triggering, and "navigator" based compensation (16).

Averaging

Like ECG, signals from external respiratory sensors such as bellows can be used to gate the acquisition to respiration. The combination of respiratory and cardiac gating can dramatically prolong acquisition time. Alternatively, respiratory motion artifacts can be minimized via averaging acquisitions over multiple respiratory cycles. While averaging results in improved SNR and is simple to implement, it prolongs acquisition time, and introduces motion induced blurring in the final images.

Respiratory ordered phase encoding (ROPE)

In ROPE method (17,18), the order in which phase encoding steps are acquired is governed by respiratory phase. For example, peripheries of *k*-space may be acquired during inspiration, and the central portions of *k*-space may be timed to occur during expiration. This approach minimizes the image artifacts arising from the drastic amplitude and phase variations between adjacent phase encoding steps.

Navigator echoes

Recent methodological advances permit respiratory motion artifact reduction using the so-called "navigator" based techniques. During each heart beat two types of data are collected-data that is required to form an MR image as well as some reference data indicating the position of the heart or diaphragm (19). The reference data, often referred to as navigator echo data, is acquired very rapidly immediately before (and after) acquiring the imaging data. The navigator data indicates the respiratory position of the heart (or diaphragm as a surrogate for detecting cardiac motion) immediately before the data acquisition. If the position of the heart is far away from a user prescribed reference position (e.g., end expiration), then the imaging data collected during that RR interval is automatically discarded. If the position of the heart is within the prescribed reference position, then the data acquired during that RR interval is accepted, and the next set of phase encoding steps are collected. While the navigator based methods are time consuming and technologically challenging to implement, they have found a clinical niche for obtaining high spatial resolution images of the heart and vascular system (20-22).

Minimizing flow artifacts

Flow artifacts arise either due to motion of spins in the temporal interval between RF excitation and signal readout (intra-view motion), or due to variation in blood flow amplitude between successive phase encoding steps (inter-view motion). In the case of *intra-view motion*, the relative change in the position of the moving spins between the phase encoding and measurement encoding gradient can result in spatial misregistration of such flowing spins. Intra-view motion artifacts can be partly minimized by additional gradients that render them insensitive to such motion (23,24), at the cost of slight increase in minimum attainable TE.

In the case of *inter-view* motion, rhythmic pulsation of the heart transports variable amount of blood across the imaged slice during the cardiac cycle. If the TR of the pulse sequence and the RR interval are not synchronized, then there can be substantial variation in the magnitude of MR signal across the phase encoding steps. This variation can cause periodic ghosting artifacts in the reconstructed image along the phase encoding direction (25). Such inter-view motion artifacts can be suppressed by selectively exciting and dephasing these flowing protons before they enter the slice of interest. Such spatial pre-saturation effectively diminishes the signal intensity modulation of flowing spins (25).

Assessment of cardiovascular function

Multi-phase *gradient echo* based cine cardiac imaging techniques with prospective cardiac gating are routinely used to assess global and regional cardiovascular function. In a typical gradient-echo sequence, the initial RF excitation

pulse tips M_Z by less than 90º, and the resulting transverse magnetization (M_{XY}) is then refocused by switching magnetic field gradients to form an echo. The residual M_Z makes it possible to apply another excitation pulse at short TR intervals (few ms apart). Unlike a SE, with gradient refocusing, background field inhomogeneities are not compensated, and M_{XY} decays at a faster rate, quantified by a time constant, T_2*. Therefore, images acquired with gradient echo based methods are susceptible to artifacts in the presence of metallic implants. Gradient-echo sequences provide several mechanisms to alter contrast by adjusting TR, TE, flip angle, and controlling how the residual transverse magnetization at the end of each TR is handled. Cardiac gated gradient-echo based cine imaging sequences are routinely used for assessing global and regional function of the heart, and for the qualitative evaluation of valvular function.

Assessment of global and regional ventricular function: technical considerations

Sequence: cine spoiled gradient-echo

In conventional gradient-echo based techniques, M_{XY} that is present at the end of each TR is destroyed either via RF spoiling, or gradient spoiling. Therefore, the measured signal intensity present represents the extent of M_{XY} created at each RF excitation. Inflow of fresh spins into the imaging plane yields greater signal than from static spins that have experienced multiple RF pulses. Because blood signal appears bright in these images, gradient-echo based techniques have been referred to as "*bright blood*" sequences. Such sequences typically provide T_1 weighting, and are often referred to by acronyms such as "spoiled" gradient-echo (Sp-GRE), or T_1-Fast Field Echo, or Fast Low Angle Shot (FLASH) (26,27).

The basic methodology for using gradient-echo based techniques for assessing global ventricular function is best illustrated with an example. Let us consider using cine TFE sequence with a TR of 5 ms for assessing the LV function of a patient with a HR of 60 bpm at a temporal resolution of 50 ms and a matrix size of 128×128. The first ten phase encoding steps (50 ms duration) will be repeated continuously throughout the first RR interval, and during the second RR interval, the next ten phase encoding steps will be acquired repeatedly throughout the cardiac cycle. Thus, in 13 RR intervals, all phase encoding steps necessary to make an image at each cardiac phase will be collected (20 phases × 128 phase encoding/phase). Then, separate images will be reconstructed using the data acquired at each temporal position and played in a "cine" loop providing detailed information about cardiac wall motion. A series of slices are acquired to cover the entire heart, and from this both volumetric information as well as functional information about the heart can be quantitatively evaluated without geometric assumptions.

While gradient echo methods are easy to implement and widely available, there are some notable shortcomings. The ebb and flow of spins into the slice of interest during diastole and systole results in blood signal intensity variation across the cardiac cycle. While intra-view flow compensation could partly mitigate this issue, incorporating such tactic prolongs the TE and lowers attainable temporal resolution or prolongs breathholding time. Furthermore, slowly flowing spins hugging the walls of the heart chambers experience many more RF pulses and the resulting reduction in their signal intensity may lead to overestimation of wall thickness.

Sequence: cine-echo planar imaging (EPI)

Transverse magnetization created following RF excitation may be encoded into several phase encoding steps by repeated refocusing to form echoes via gradient alternations. Such EPI readouts can offer dramatic improvements in temporal resolution, by spreading the temporal overhead associated with the slice selection process across multiple phase encoding steps. The main drawback of using an EPI readout is the prolongation of TE and the increased sensitivity to oblique and turbulent flow, as well as magnetic field inhomogeneities induced by metallic implants etc. (28-30). However, in some instances this increased sensitivity to flow disturbance can be used advantageously for identifying trace regurgitation, or disturbed flow through a stenotic valve, that may not otherwise be obvious (*Figure 2*). However, it is important to realize that such identification through EPI based techniques is qualitative.

Sequence: cine-balanced steady state free precession sequence

Unlike Sp-GRE, in balanced steady-state free precession (SSFP) sequences (7,31) the phase coherence of residual transverse magnetization at the end of each TR is carefully preserved by nulling the total gradient areas under all three encoding directions over TR. This leads to coherent accumulation of signal towards a steady state value. SSFP sequences demand high field homogeneity to maintain steady state, and is necessary to have a TR << T_1 or T_2, so that background field variations do not disrupt the spin

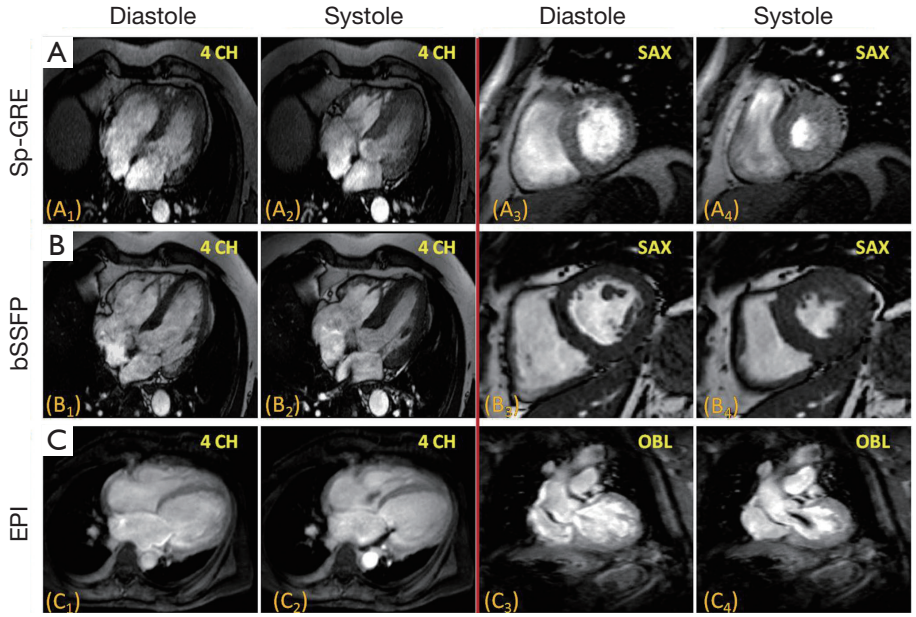

Figure 2 Representative images from cine sequences obtained with spoiled fast gradient echo (A), balanced SSFP (B), and echo-planar imaging (C) sequences are shown-at systole and diastole. Note the relatively high blood-to-muscle contrast of the SSFP sequences compared to the spoiled gradient echo or EPI cine images. The long TE of EPI cine sequences makes it possible to visualize flow disturbance caused by valvular regurgitation (C). SSFP, steady state free precession; EPI, echo planar imaging.

phase coherence. Unlike conventional sequences, which are either T_1 or T_2 or PD weighted, the resulting steady state signal is proportional to the T_2/T_1 ratio of the tissues. In the case of cine imaging of the heart, this contrast behavior is particularly desirable as the T_2/T_1 ratio of blood is substantially higher than the T_2/T_1 ratio of myocardium. As a result, SSFP sequences provide very high intrinsic contrast between blood and myocardium (*Figures 2B,3*) with high SNR. Moreover, as the gradient waveforms are perfectly balanced at the end of each TR, this sequence is intrinsically flow compensated along the frequency encoding direction, thus limiting flow induced signal loss. Lastly, unlike conventional cine gradient-echo sequences, the SSFP sequence does not rely on "*in-flow*" of fresh spins for generating contrast and provides uniform blood signal intensity throughout the cardiac cycle. Compared to conventional Sp-GRE sequences, SSFP sequences offer better contrast resolution, higher SNR, lesser dependence on flow related artifacts, and is the sequence of choice for evaluating global and regional function of the heart (32).

Assessment of cardiac function: clinical applications

MRI has a distinct advantage for cardiac chamber volume determination as it is not dependent on geometric models and assumptions that can alter the accuracy of planar imaging techniques, such as contrast ventriculography, or those with limited imaging planes, such as echocardiography (33,34). The complex shape of the RV defies simple geometric models, and MR is uniquely suited to measure RV volumes. Using a complete set of MR images through the entire heart, either in short-axis or transaxial projections, chamber wall, and cavity volumes at all anatomic levels can be measured and summed for direct calculation of right- and left-heart chamber dimensions (*Figure 2*). In normal volunteers, measurements of stroke volume (SV) for the RV and left ventricle (LV) derived from the sum of cavity volumes at end-diastole and end-systole shown on multiple contiguous transaxial images have been nearly identical (35,36).

SE and cine-MRI can be used to reproducibly acquire static and dynamic images with low intra-observer and inter-observer variability (37-41). However, multilevel cine gradient-echo techniques are now the norm for left and right ventricular analysis. Initial work measuring LV end-diastolic and end-systolic volumes (ESV) and ejection fraction (EF) have correlated well with EF values from contrast ventriculography (40,41). The reproducibility of measurements of ventricular dimensions obtained with

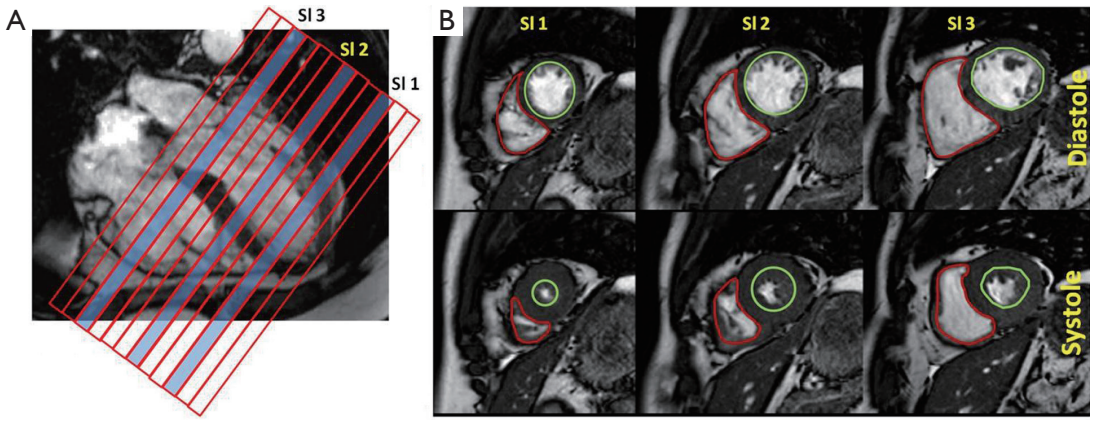

Figure 3 Cine balanced steady-state free precession (SSFP) images are routinely used for ventricular volumetry, due to their high blood-to-myocardial contrast, and SNR. For LV and RV volume quantification, a stack of short axis slices (~8 mm slice thickness) covering both the ventricles from the base of the heart to the apex is obtained (A); (B) shows representative images from the stack at three different locations, and at systole and diastole. Contours demarcating the LV and RV cavity are drawn at end-systole and end-diastole for all the slices. The areas are summed to obtain the end-diastolic volume (EDV), end-systolic volume (ESV). From EDV, and ESV, the stroke volume (SV = EDV – ESV), and ejection fraction (EF = SV/EDV*100) are calculated.

short axis cine-MRI has been assessed with small inter-study variability in the measurements of LV mass, end-diastolic and ESV, and EF (39,42). Moreover, cine-MRI has significantly smaller variability in measurements than echocardiography. This feature makes CMRI the optimal technique for precise measurement of LV mass and volumes over time—a factor that makes CMRI particularly advantageous for monitoring therapeutic interventions and LV remodeling (43,44). Furthermore, the high-soft tissue contrast of CMR permits quantitative assessment of regional wall motion by drawing epi- and endo-cardial contours, during both diastole and systole.

Assessment of cardiovascular morphology

In this section, we will briefly describe commonly used MR methods to visualize cardiovascular morphology. Most commonly used cardiac morphologic imaging methods are the so-called "black-blood", imaging methods. In these techniques, blood signal is suppressed to highlight myocardial, valvular, and vascular structures. Pathologic processes can significantly alter tissue MR properties T_1, T_2, T_2*, etc. For example, significant accumulation of fat, edematous changes following acute insults or deposition of iron can result in measurable changes in tissue T_1, T_2, and T_2* respectively. It is common practice to adapt morphologic imaging methods to provide tissue characterization information.

Assessment of cardiovascular morphology: technical considerations

Sequence: spin-echo (SE) based black blood imaging

In SE, the initial transverse magnetization created by 90° excitation pulse is refocused using a 180° refocusing pulse, to form an echo at a prescribed echo time (TE). The data acquisition window is typically selected to coincide the quiescent period of the cardiac cycle such as mid or end diastole, and the basic module of 90°-180° RF pulses is used to create a SE. The mechanism of generating black blood appearance is described in *Figure 4*. The absence of signal for flowing spins is most pronounced only when the slices are oriented perpendicular to the direction of flow, and the flow velocities are high enough to be transported out of the slice in the duration between the 90° and 180° pulses. Therefore, simple SE sequences do not provide adequate suppression of blood signal in oblique orientations.

Sequence: dual inversion recovery black-blood (DIR-BB) sequence

A commonly used clinical black-blood imaging method that overcomes many of the limitations of the conventional SE based techniques is the so-called *DIR-BB imaging* method (45). In DIR-BB preparation, a non-selective 180° pulse and another inversion pulse that selectively inverts the slice of interest are applied in rapid succession. The combined effect of the non-selective, selective 180°

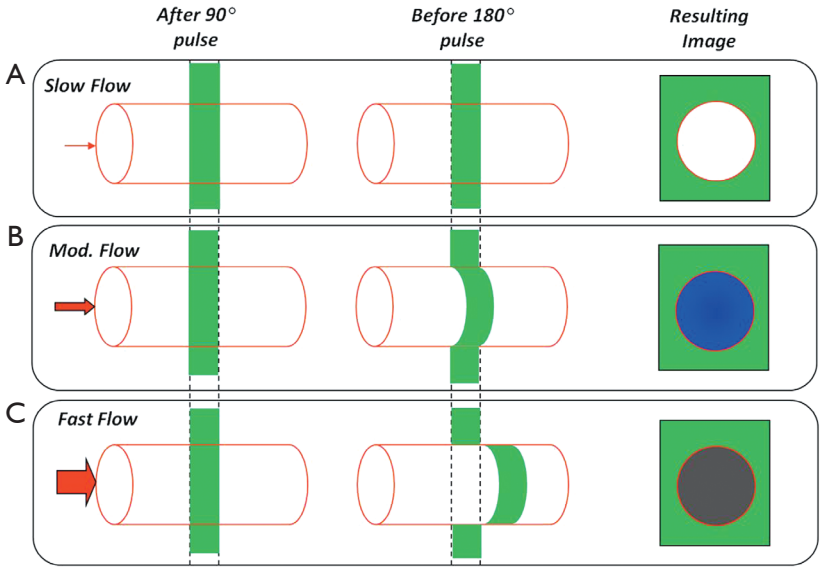

Figure 4 Spin echo based black-blood imaging based on time-of-flight (TOF) phenomenon. Through plane flow through a slice at different flow rates, slowest on the top panel and the fastest in the bottom panel. Slow flowing spins experience both the 90° and the 180° pulses, and therefore fully refocus to give a bright signal (top panel). On the other hand, if the spin velocity is high enough, none of the spins experience both the 90° and the 180° pulses resulting in a signal void within the vessel (bottom panel). If the spin velocity is in-between these two extremes, then the resulting image has a signal intensity that is proportional to the fraction of the spins that experienced both the 90° and the 180° RF pulses (middle panel). As a result slowly flowing spins near the vessel wall can refocus and make the vessel wall appear thicker, if the TE is too short.

pulse pair is to invert all spins outside the slice of interest. Therefore, one can eliminate the contribution of blood signal from outside the slice of interest if a 90° pulse is applied to the slice at a time when the inverted blood signal outside the slice crosses zero. The blood that was inside the slice of interest is expelled from the slice due to cardiac systole that occurs in the interval between the DIR preparation and the measurement. As a result, an anatomic image of the heart that is devoid of signal from blood ('black-blood') is obtained. Unlike simple SE based BB imaging techniques, DIR-BB imaging technique is independent of the orientation of the slice with respect to flow (*Figures 5,6*). DIR-BB TSE sequence parameters can be modified to produce images of varying contrast. For example, choosing a longer TE (~70-80 ms, turbo factor of 16-24/shot), and a longer TR (>2,000 ms, 2-3 RR intervals between 90° pulses) results in a T_2 weighted DIR-BB image.

Sequence: modifications to DIR-BB sequences

BB preparation pulse module (i.e., double-inversion pulse pair) is often combined with another slice selective IR pulse (46), to provide fat suppression in addition to blood signal suppression (*Figure 5*). This so-called *triple-IR* sequence is often used to visualize inflammation of vascular structures (47) or myocardium in the setting of acute myocardial infarction.

DIR-BB and triple-IR preparations are used to null signal from one specific tissue (blood), and two specific tissues (blood and fat) respectively. This principle can be extended to null signal from tissues with a range of T_1 values. For example, a pair of dual inversion (so called, Quad-IR) preparation pulses can be used to null signal from tissues spanning a range of T_1 values. Quad IR (48,49) prepared sequences have been used to visualize plaque in carotid arteries before and after contrast administration without the confounding effects of blood signal. Other common modifications include the additional application of spectrally selective RF pulses (ChemSAT) in the interval between the DIR preparation and the turbo-SE readout to suppress signal from fat. Such fat suppressed, high resolution T_2 weighted DIR-BB TSE sequences have also been used to visualize plaque in carotids (49), and for the visualization of coronary arteries (50).

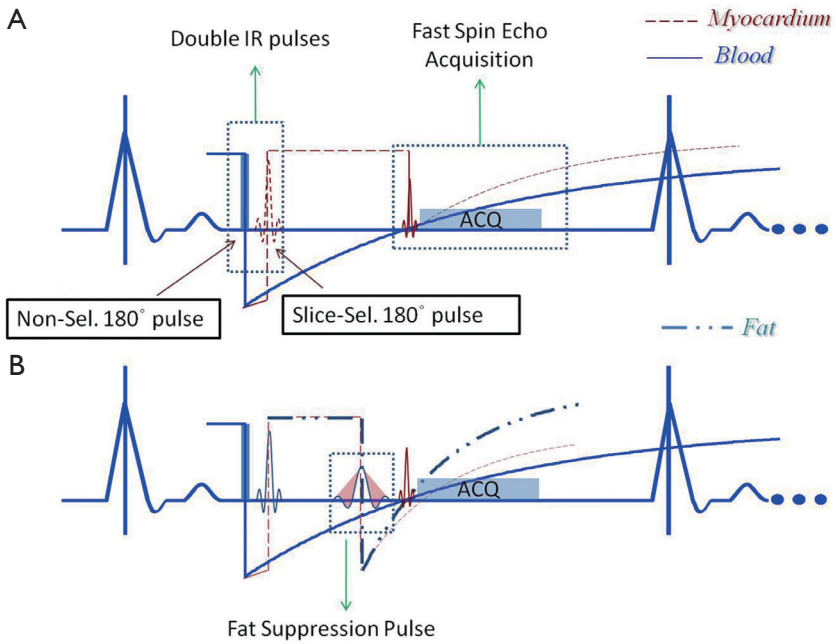

Figure 5 A schematic of the dual inversion recovery black blood (DIR-BB) pulse sequence is shown in A and in B (with an additional pulse for fat suppression). In (A) after the occurrence of the RR wave, two 180º pulses are applied. The first pulse is a non-selective pulse that inverts the magnetization of all the spins in the body. The second 180º pulse selectively re-inverts the spins in the slice of interest. When the blood magnetization approaches zero, a fast spin echo read-out is performed to obtain the BB-DIR image. When additional fat suppression is desired, an additional inversion pulse to suppress the fat signal can be applied as shown in (B) In this instance, the TI is chosen to suppress signal from blood as well as fat signal.

Technical limitations of DIR-BB T_2 weighted imaging

The main technical limitations of T_2-weighted imaging are (51): (I) bright signal intensity caused by slowly flowing blood near the vessel wall, or chamber walls, can mimic inflammation; (II) potential mis-registration due to tissue motion in the relatively long TI (~600 ms) interval between the DIR preparation and the TSE readout which can cause myocardial signal loss (hyperkinetic LV) in otherwise normal LV. These signal intensity variations in T_2 weighted DIR-TSE sequences make it difficult to use myocardial signal intensity as a robust marker of underlying pathology. Improved imaging sequences (52,53) and quantitative T_2 measurements (54) may overcome some of these limitations.

Assessment of cardiovascular morphology: clinical applications

Multi-slice simple SE sequences are typically acquired as transverse slices to provide global perspective of the relationships of the cardiac chambers, great vessels, and adjacent structures, but are of limited value in accurately measuring chamber sizes and volumes (55,56). In transverse imaging, for example, the region of the LV adjacent to the diaphragm is obscured due to volume averaging with the adjacent diaphragm, as it is sliced tangentially, and it is necessary to visualize the heart in at least two orthogonal orientations (57).

Breath held DIR-BB techniques can provide images with exquisite soft-tissue contrast are of particular value in the evaluation of LV and RV cardiomyopathies. DIR-BB sequences are clinically used to assess the extent of myocardial injury in the setting of acute myocardial infarction, or for identifying vascular inflammation. Furthermore, pre- and post-contrast T_1 weighted images are routinely used in clinical practice to assess cardiac masses. Chemical shift selective excitation pulses, added to DIR-BB sequences, can provide useful information in the clinical evaluation of fatty masses or fatty infiltration in the myocardium.

Assessment of blood flow

As discussed in the previous two sections, the inflow and outflow of blood play a crucial role in determining the

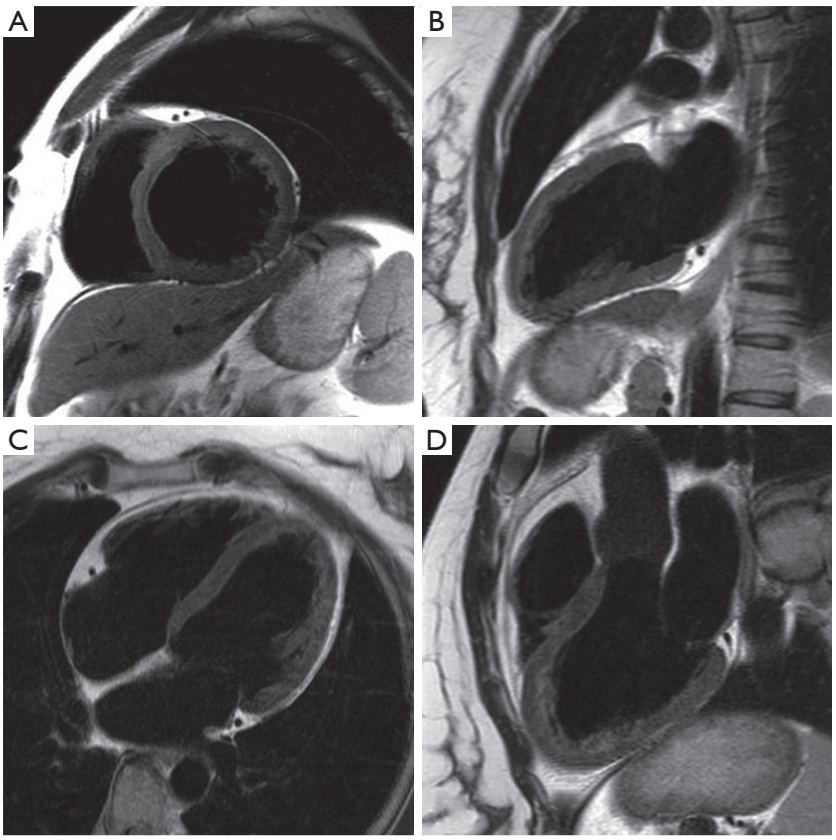

Figure 6 Representative black blood images of the heart in the short-axis (A), vertical long axis (B), 4-chamber (C) and left ventricular outflow tract (D) views are shown in this figure. Notice effective nulling of blood independent of the orientation of the acquisition.

blood-myocardial contrast in the bright blood and black-blood sequences. Blood flow across stenotic and regurgitant valves is turbulent, and results in flow induced dephasing. In cine turbo field echo sequences, this flow induced dephasing can be made more conspicuous by deliberately choosing a longer TE (*Figure 2C*), providing a qualitative evaluation of the valvular dysfunction. MR also provides a way to quantify blood flow using a technique called phase-contrast imaging.

Principle of phase-contrast velocity mapping

The amplitude of the measured transverse magnetization (M_{XY}) or MR signal depends on the interplay between tissue specific parameters (T_1, T_2, PD etc.), and MR acquisition parameters (sequence type, TR/TE, etc.). As MR signal is complex, the phase of the MR signal is influenced by factors such as local susceptibility, spin velocity etc. In MR phase-contrast velocity mapping (PVM), the phase of the MR signal is manipulated to yield information about spin velocity.

The proton precessional frequency modulated by the superposition of magnetic field gradients is used to encode spatial position of spins. By adding an additional gradient waveform within the imaging sequence, e.g., bipolar gradient, it is possible to encode spin velocity. Such velocity encoding allows a spin moving in the direction of the magnetic field gradient to accumulate a net phase shift compared to a static spin (*Figure 7*), and the phase shift can be directly related to the velocity (v) of the spin using the following relationship (58):

$$\phi = \gamma M_1 v,$$

where γ is s 42.57 MHz/Tesla for protons, M_1 is the first temporal moment—an operator controlled variable that is a function of the strength, shape, duration, and the temporal position of the motion-encoding gradient waveform within the imaging sequence—given by:

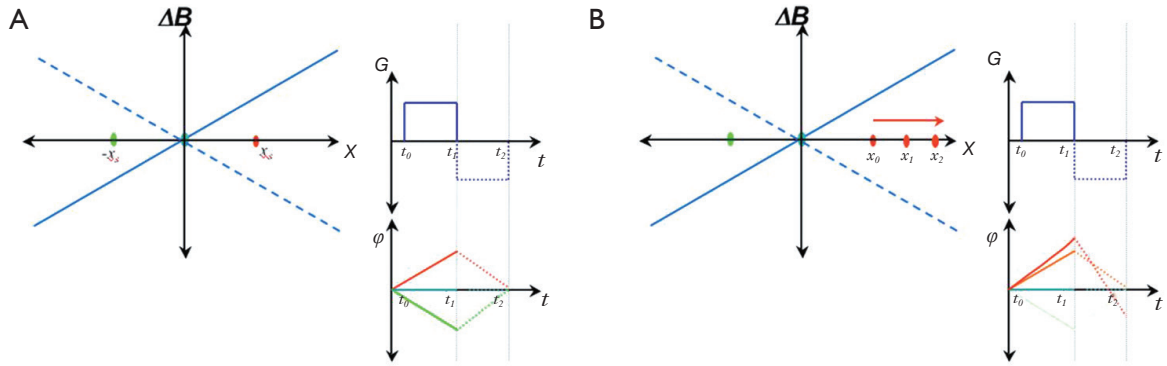

Figure 7 (A) *Effect of bipolar gradient on static spins*: on the left, the field variation imposed by the bipolar gradient is shown schematically. The solid blue line indicates the field gradient between time points t_0 and t_1, and the dotted blue line indicated the field gradient between time point t_1 and t_2. The bipolar gradient waveform is shown on the right, and the corresponding phase evolution diagram during the course of the gradient is shown below. A spin located at the iso center (cyan color) experiences no net additional field, and as a result accumulates no phase shift. Let us consider the case of a spin at location x_s (red color). This spin experiences a slightly higher magnetic field during the positive lobe of the bipolar gradient between time points t_0 and t_1, and during this time accumulates a net positive phase shift (with respect to a spin at the iso center). When the gradient polarity is reversed during time interval t_1 and t_2, the same spin experiences a slightly lower magnetic field strength, and starts to accumulate a negative phase shift. At the end of the bipolar gradient lobe, the spin at location x_s, accumulates no net phase shift. By the same argument, it is easy to see that static spins do not accumulate a net phase shift independent of their location along the X-axis; (B) *Effect of bipolar gradient on moving spins*: let us consider a spin at location x_0 at time point t_0 that moves at a constant velocity. Between time points t_0 and t_1, the moving spin traverses through an ever increasing magnetic field strength as shown on the left. Compared to a static spin at location x_0, by virtue of its motion from location x_0 to x_1 in the presence of the positive lobe of the bipolar gradient oriented along X, the spin accumulates a slightly higher phase at time point t_1. As the gradient polarity is reversed at time point t_1, the spin starts to accumulate a negative phase shift. As the spin continues to move from x_1 to x_2 under the influence of the negative lobe of the bipolar gradient, the rate of phase accumulation is even greater, as the spin experiences a much higher negative magnetic field strength. At the end of time point t_2, unlike a static spin, the moving spin accumulates a net negative phase shift. By the same argument, it is easy to show that spins moving in the opposite direction at the same rate would accumulate a net positive phase shift under the influence of the same bipolar gradient. Thus, moving spins accumulate a phase shift that gives information both about the rate of displacement, as well as the direction of motion. This phase accumulation forms the basis of phase contrast measurements in MRI.

$$M_1 = \int_0^{TE} t.G\,(t)\,dt$$

To eliminate the confounding influence of background phase shifts caused by phenomena unrelated to spin velocity, MR-PVM typically acquires two sets of otherwise identical data in which the polarity of the motion encoding gradient is alternated. Phase difference images generated from the two acquisitions provides information regarding the spin velocity.

It is also important to note that the induced phase shift is proportional only to the component of velocity along the direction of the magnetic field gradient, and phase is sensitive to direction of flow along the gradient waveform (*Figure 8*). Therefore, to measure the true velocity, it is necessary to either align the velocity encoding direction in the direction of flow or measure all three components of the velocity vector by superimposing gradients along all three orthogonal directions.

Assessment of blood flow: technical considerations

Strength of velocity encoding

As discussed above, motion induced phase shift is proportional both to spin velocity v, as well as M_1 used in the pulse sequence. For a given spin velocity, by adjusting M_1, it is possible to induce a very large or a very small phase change in the signal. The phase-contrast velocity measurements are chosen such that the maximum velocity within the slice of interest induces a phase shift less than 180°. This limiting value of the strength of the velocity

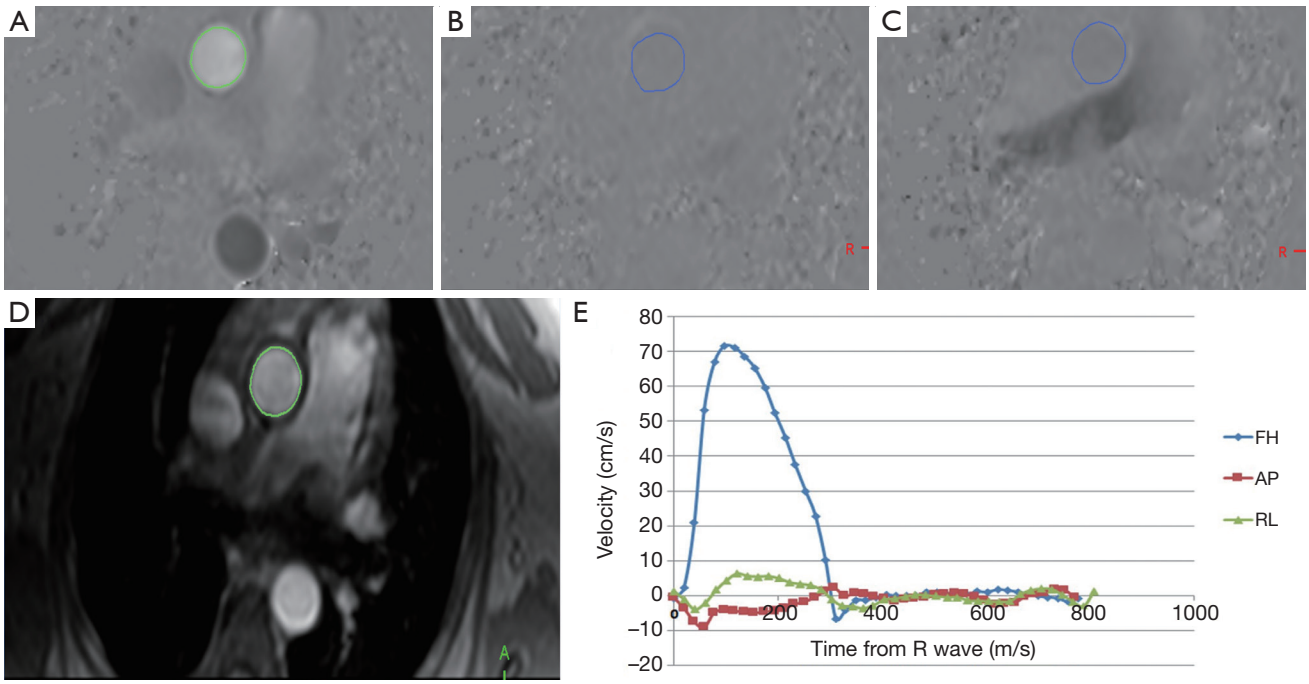

Figure 8 Complete evaluation of the velocity vector components by superimposing velocity-encoding gradients along each of the three orthogonal axes. A single frame of the phase contrast image (showing the ascending aorta) obtained with velocity-encoding gradients along the FH (red), AP (green), and RL (brown) directions is shown in (A), (B), and (C) respectively; the magnitude image that provides anatomic information can be readily reconstructed from the phase contrast measurement data (D); the average velocity across the vessel along the RL, FH, and AP during the cardiac cycle is shown in (E). It is seen that most of the flow exists along the FH direction with minimal flow occurring in the AP and RL directions.

encoding is often referred to as the V_{enc} value. Any velocities greater than the V_{enc} value within the slice of interest appear as artifically lower velocities flowing in the other direction—a phenomenon referred to as aliasing. Because the standard deviation of the measured velocity is proportional to the V_{enc} value, the V_{enc} value should be chosen just high enough to avoid velocity aliasing in the vessel of interest (59).

Strategies for velocity encoding

As discussed above, two complete sets of measurements are sufficient to measure a single component of the velocity vector using PVM. A simple extension of this approach to fully resolve the velocity vector would result in tripling of the acquisition time (59,60). An alternative is to use one reference acquisition, and three velocity encoded acquisitions, resulting in a total of four measurements or doubling of time compared to the two-point, unidirectional velocity measurement (*Figure 4*). However, in this case, it is important to note that as a single reference scan is used for all three velocity encoded images, the noise in the images is correlated (59).

Type of cardiac gating

In prospective gating methods, the MR spectrometer waits for the ECG trigger to occur (usually identified by the top of the R wave), before commencing data acquisition across the cardiac cycle (typically about 80-90 percent of the RR interval). Therefore, missing 10-20% of diastole can result in substantial underestimation of the severity of aortic/pulmonary regurgitation. To avoid this underestimation, it is common practice to use retrospective gating for clinical PVM in the evaluation of aortic regurgitation. It is also common to average the PVM data to minimize errors introduced by other undesired forms of motion. The main disadvantage of the retrospective gating, and averaging is the prolonged acquisition time (~2-3 min per slice per velocity encoding direction). While, recent advances in segmented *k*-space acquisitions permit much faster acquisition, they should be used with care as they can

introduce spurious phase shifts due to eddy currents, and other hardware related effects.

Through-plane versus in-plane velocity encoding

Quantitative flow measurements are typically performed by prescribing the velocity encoding gradient on the slice encoding direction. This permits the simultaneous evaluation of both the mean blood velocity across the vessel, as well as the area of the vessel, so as to quantify blood flow across the vessel (61).

Estimation of peak velocities (v_m) of stenotic jets is clinically important and can be used to estimate the pressure gradient (ΔP) using the simplified Bernoulli's equation: $\Delta P = Kv^2$, where K is the loss constant usually assumed to be four. For the purposes of visualizing and quantifying peak velocities in stenotic jets, it is advantageous to encode for velocities in the plane of the jet. However, such in-plane velocity encoding is fraught with several challenges. First, the dimension of the voxel in the slice direction is typically about two to three times longer than in the in-plane encoding directions. Therefore, peak velocities of small jets (comparable to the slice thickness) suffer from significant underestimation due to partial-volume averaging. Secondly, the turbulent jet may not lie in one plane, and it may be necessary to encode for velocities in more than one direction. Lastly, with through-plane velocity encoding, if it is of interest to measure the peak velocity, it is important to position the imaging slice across the location of maximum velocity, and this may be difficult to determine *a priori*. Often, the peak velocity profile of the jet can extend up to five times the diameter of the jet within the imaging plane, allowing some margin for accurate slice placement. In general, the location of the phase contrast imaging slice can have a major influence on the accuracy of measurements, not only on peak velocity estimation, but also on the estimation of regurgitation (62,63).

Partial volume effect

Partial volume effects (mixing of static and moving spins) can significantly underestimate the PC-MRI measurements in a number of ways. Partial volume errors occur when: (I) if the slice of interest intersects the vessel of interest non-orthogonally, and the extent of error is proportional to the ratio of voxel size to vessel size; (II) the thickness of the prescribed slice is comparable to the size of the jet being evaluated (underestimation of peak velocity). Studies have shown that it is necessary to have roughly four pixels across the diameter of the vessel of interest (or around 14 voxels across the cross-section of the lumen) to have errors less than 10% (64-67).

To minimize the error associated with the measurement of peak velocity from a single pixel, some studies have suggested that an average of four pixels in the central core of the jet may be used. It should also be remembered that MR measurements of peak velocities are time averaged values, and in general, are lower than instantaneous measurements of velocity often reported in echo-cardiography.

Assessment of blood flow: clinical applications

PVM provides an effective way to measure both regurgitation as well as stenosis across valvular structures in the heart. Some clinical examples of using PVM for the measurement of valvular regurgitation and stenosis are shown in *Figures 8* and *9*. Progressive dilation of the ventricular chamber volume in the presence of clinically significant regurgitation can be estimated from conventional cine imaging. Similarly, thickening of the ventricular chambers in the presence of clinically significant stenosis can also be measured using cardiac cine imaging. Therefore, the combined ability to measure global ventricular function via cine imaging, as well the ability to measure blood velocities (and flow) across valvular structures along any orientation makes MR a powerful tool in the evaluation of valvular diseases.

Assessment of ischemia, myocardial viability, and coronary anatomy

Assessment of ischemia

Myocardial perfusion reserve is a sensitive index for assessing myocardial ischemia. Perfusion scans for the assessment of ischemia are performed under conditions of rest and repeated with pharmacologic vasodilator stress. According to the "ischemic cascade" theory, when a significant coronary artery stenosis is present, a perfusion abnormality will occur before diastolic dysfunction and regional wall-motion abnormalities arise; these developments are followed by electrocardiographic ST-segment changes and, finally, the onset of chest pain (68). Vasodilators such as adenosine and regadenoson act on the A_{2A} receptor. They increase myocardial blood flow (MBF) in normal coronary arteries by causing smooth muscle relaxation and vascular dilation; however, coronary arteries that have a significant stenosis show little or no increase in blood flow on exposure to these vasodilators. The resulting flow heterogeneity produces a steal phenomenon (69), which manifests as a perfusion

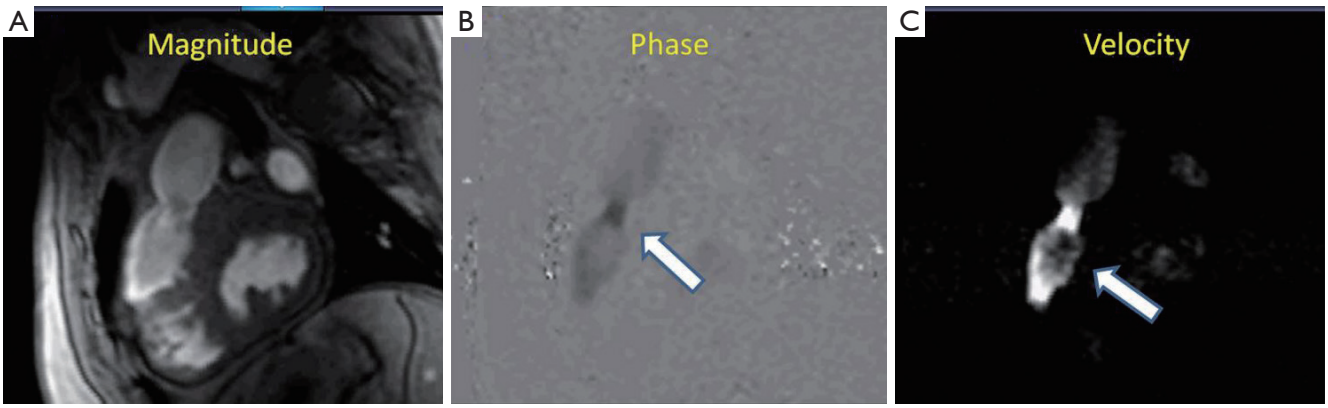

Figure 9 Valvular regurgitation across the RV outflow tract. (A) Magnitude images do not conclusively demonstrate flow disturbances across the valve; (B) the phase images (white arrow) show a hypo intense region just after the valves close, reflecting to a phase turbulence occurring due to the regurgitation; (C) the velocity images (white arrow) also demonstrate the same.

defect during stress perfusion and resolves during rest perfusion if critical coronary stenosis is not present. A typical stress perfusion protocol involves rapid administration of gadolinium based contrast agent (GBCA) (0.05-0.1 mmol/kg at 3-4 cc/s) during peak pharmacologic stress (approximately one minute after administration of a 400 mcg intravenous bolus of regadenoson or three minutes after administration of a 140 mcg/kg/min intravenous infusion of adenosine). The relatively low dose of Gd is used to ensure a linear relationship between MR signal intensity and contrast concentration, without the confounding effects of T_2* related signal loss (70).

Assessment of ischemia: technical considerations

During the first passage of the contrast agent, a series of ECG triggered, T_1-weighted gradient-echo images of the heart are acquired each heart beat to study the first pass kinetics of GBCAs. These images are acquired in diastole, and T_1 weighting is enhanced by the application of additional preparatory RF pulses. A commonly used T_1 preparation pulse is a 90° excitation pulse which renders the sequence insensitive to arrhythmias. The signal is acquired using a series of gradient-echoes following the magnetization preparation delay to enhance T_1 weighting. As the contrast agent perfuses the myocardium, T_1 of the myocardium is substantially shortened. This T_1 shortening causes an increase in signal intensity in the resulting images early in the passage of contrast (wash-in phase), and as the contrast agent mixes with the blood pool over time, the signal intensity is reduced (wash-out phase) (*Figure 10*).

For each pixel or region of myocardium signal intensity curves can be generated as a function of time. From these time intensity curves wash-in and wash-out rates can be estimated. It should be noted that bulk of the GBCAs approved for clinical use are extravascular, and readily leak from the intra-vascular space to the interstitial space. Consequently, the myocardial signal enhancement is not a simple function of perfusion, but also depends on tissue blood volume, size of extravascular compartment, and the degree of capillary permeability. Therefore, attempts to quantify myocardial perfusion should take these confounding effects into consideration. Most clinical perfusion studies are evaluated by either semi-quantitative or visual analysis of MR images. Semi-quantitative analysis methods typically use a metric such as the ratio of the up-slopes (rest over stress studies normalized by the LV blood-pool signal) (71,72). However, it is possible to estimate absolute quantification of myocardial flow using sophisticated analysis methods, and readers are referred to several excellent previously published review articles (73-76).

The main limitation of the MRI based myocardial perfusion imaging sequence is the need for faster data acquisition to improve coverage without compromising spatial, temporal or contrast resolution. Several rapid imaging methods that use EPI based acquisitions (reducing effective TR) or using SSFP readouts (75,77,78), sharing the pre-pulse across slices, parallel imaging methods that exploit spatio-temporal correlations (79-81), etc. are actively being considered by many groups. This is a promising and an active area of research (81).

Assessment of ischemia: clinical application

From a clinical point of view, several studies have evaluated

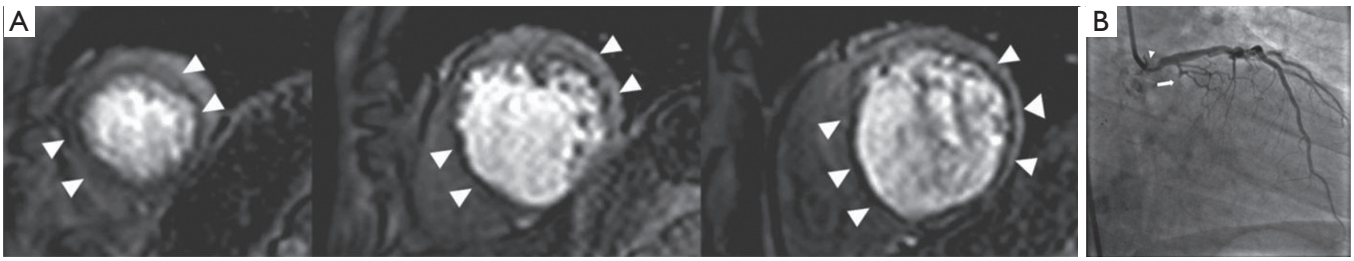

Figure 10 Vasodilator stress perfusion cardiac magnetic resonance image and the corresponding invasive angiogram. Images are from a 68-year-old man who presented with chest pain. (A) Stress perfusion study using adenosine revealed reversible hypo-perfusion involving the left anterior descending (arrowheads) and left circumflex territories (arrowheads) (rest perfusion not shown). From left to right: the apical-, mid- and basal-third of the left ventricle; (B) invasive angiography revealed a significant left main lesion (arrow) and an occluded left circumflex artery (arrowhead).

the diagnostic performance of CMRI to detect myocardial ischemia. Recently published results from the MR-IMPACT II study (82) with 515 patients, showed that perfusion CMRI had a higher sensitivity than SPECT (0.67 *vs.* 0.59, respectively) but a lower specificity (0.61 *vs.* 0.72, respectively). A more recent study (83) with more than 600 patients found that the sensitivity, specificity, positive predictive value, and negative predictive values for CMRI were 86.5%, 83.4%, 77.2% and 90.5%, respectively, and 66.5%, 82.6%, 71.4%, and 79.1% for ECG-gated SPECT. The sensitivity and negative predictive values were significantly better for CMRI than for SPECT (P<0.0001). These studies demonstrate that CMRI perfusion can play a crucial role in the evaluation of myocardial ischemia.

Assessment of myocardial viability

MR imaging methods such as delayed-enhancement MRI (DE-MRI), use of specialized contrast agents such as ion transport agents (e.g., manganese) or necrosis-specific agents (e.g., gadophorins), CMR spectroscopy, or assessment of myocardial contractile reserve (via low-dose dobutamine) can all provide information regarding myocardial viability. In this review, we will focus on DE-MRI, the most commonly used method for assessing myocardial viability.

Myocardial viability: technical considerations

Intact cell membranes in healthy myocardium exclude extra-vascular contrast agents, whereas the loss of cell membrane integrity associated with irreversible myocardial injury increases the distribution volume for GBCAs (84). This differential distribution volume for GBCAs is exploited in DE-MRI to generate contrast between irreversibly injured and normal myocardium (85). Following GBCA administration, GBCA's such as Gd-DTPA preferentially accumulates in irreversibly injured myocardium within minutes, resulting in differential contrast lasting for up to 45 minutes or more. As a result, the T_1 of the irreversibly injured myocardium is shorter than the T_1 of normal or viable myocardium. This T_1 difference between the injured and normal myocardium is exploited, by using an IR prepared T_1 weighted gradient-echo sequence (*Figure 11*). The inversion delay is chosen such that the normal myocardial signal intensity is zero. Therefore, in these so called "delayed hyperenhancement" images, normal myocardium appears dark and irreversibly injured myocardium appears bright (*Figures 12,13*).

Myocardial viability: clinical applications

Several recent studies have demonstrated the utility of the technique in animal and human studies (71,83). In a seminal study by Kim and colleagues (6), DE-MRI was able to identify dysfunctional but viable myocardium and predict functional recovery after coronary revascularization. In that study, approximately 80% of the dysfunctional segments with fully viable myocardium showed improvement in functionality after revascularization, whereas only 10% of the segments with 51% to 75% hyper-enhancement/scar showed functional recovery The above-mentioned findings have been confirmed by other studies (86,87).

Some of the limitations of viability assessment have been elegantly summarized in a recent article by Schinkel and colleagues as (88,89): (I) a large amount of scar tissue adjacent to viable myocardium could limit functional recovery (90); (II) in a severely dilated heart that has undergone significant remodeling, improvement may not

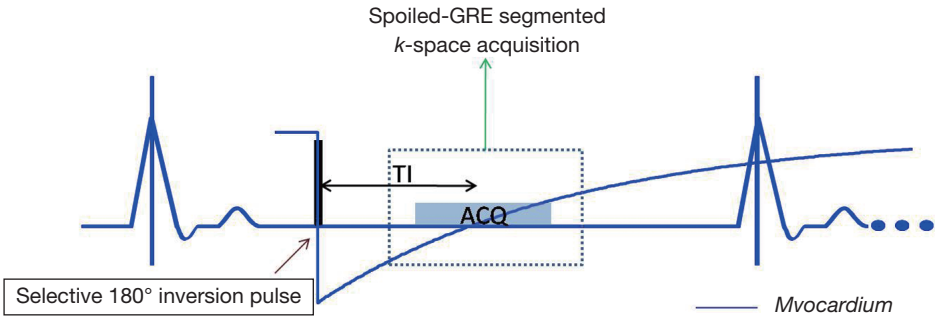

Figure 11 Inversion recovery based delayed hyper enhancement sequence for viability imaging. This sequence produces images in which the signal from myocardium is nulled—myocardium appears dark while any scar appears bright. After the R wave is encountered, an inversion pulse is applied such that myocardium is nulled at the time of acquisition. A suitable inversion time is determined by performing a TI scout sequence (e.g., Look Locker) before the actual sequence. A spoiled gradient—T_1 weighted segmented *k*-space acquisition is used to acquire the viability images.

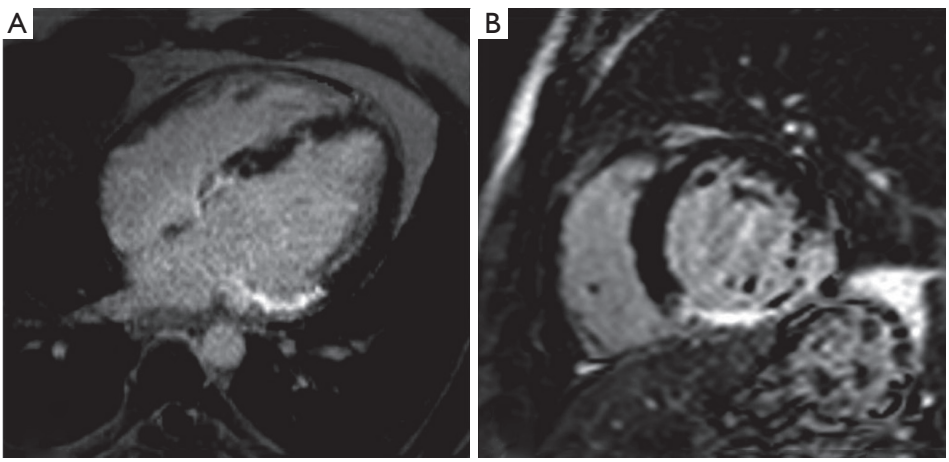

Figure 12 Delayed hyper-enhancement images in the 4-chamber (A) and the short axis views (B). After injection of an extra vascular contrast agent (Gd-DTPA), inversion recovery based T_1 weighted gradient echo images are obtained that null the signal of normal myocardium. In these images, the normal myocardium appears dark, and the scar region appears bright—due to the fact that Gd-DTPA preferentially accumulates in irreversibly injured myocardium within minutes following contrast administration, thereby decreasing the T_1 of the irreversibly injured myocardium. Note the dark circular region (panel B) surrounded by scar regions in the inferior wall (five o'clock) is characteristic of micro vascular obstruction.

be possible, despite the presence of viable myocardium (88); (III) hibernating myocardium, in which metabolism has been significantly down regulated, may no longer respond to revascularization; (IV) revascularization may have been incomplete or may have failed, or new myocardial injury may have occurred during revascularization; and (V) imaging must be performed at the correct time, because it could be as long as one year before functional recovery is seen (91,92). Since the description of the DE-MRI method, there have been numerous studies that have confirmed its reproducibility, and clinical utility in evaluating ischemic and non-ischemic injury to the myocardium. It is beyond the scope of this review to provide a more comprehensive review of other MR methods suitable for assessing myocardial viability.

Assessment of coronary anatomy

The most common cause of ischemic heart disease is epicardial coronary artery stenosis. Non-invasive

visualization of the coronary arteries has long been considered the "holy grail" of CMRI, but has remained a longstanding challenge because of the complexities of imaging small, tortuous vessels, with very high spatial resolution. In addition, coronary arteries have complex and somewhat asynchronous motion; compounding this, they are relatively stationary for only brief portions of the cardiac cycle.

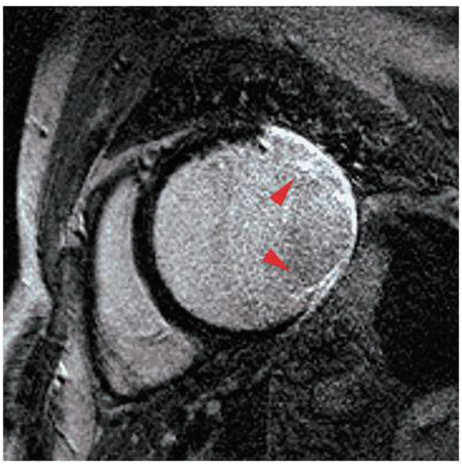

Figure 13 A short axis image at the basal location of the left ventricle is shown. The technique used is the delayed-enhancement sequence performed after gadolinium administration, which highlights the infarcted tissue as bright white, and normal myocardium as black. Note the marked thinned and bright signal intensity of the entire lateral wall from prior myocardial infarction involving the left circumflex coronary artery territory. The arrowheads denote infarction of both the anterior and posterior papillary muscles.

Assessment of coronary anatomy: technical consideration

The high spatial resolution demands in conjunction with a brief window for data collection during each cardiac cycle make the acquisition times very long limiting respiratory motion compensation strategies such as breathholding or signal averaging. Nonetheless, 3D breathholding techniques have been employed with limited success at a few centers. To date the most successful technique has been navigator echo based sequences discussed previously that are employed to minimize the effect of respiratory motion and permit visualization of coronary arteries (72). The technical description of the technique is as follows.

A high spatial resolution 3D gradient-echo volume is prescribed to cover the proximal to mid coronary arteries. A portion of the data necessary for constructing the 3D volume is acquired during each heartbeat at mid diastole, when coronary blood flow velocity is maximized. Before the data acquisition, a navigator echo is collected to verify the position of the heart. The acquired data is accepted only if the position of the heart, as determined by the navigator is within a prescribed margin. In addition, to maximize the contrast between the flowing blood and the surrounding, both as a muscle suppression pulse (T_2-preparation) as well

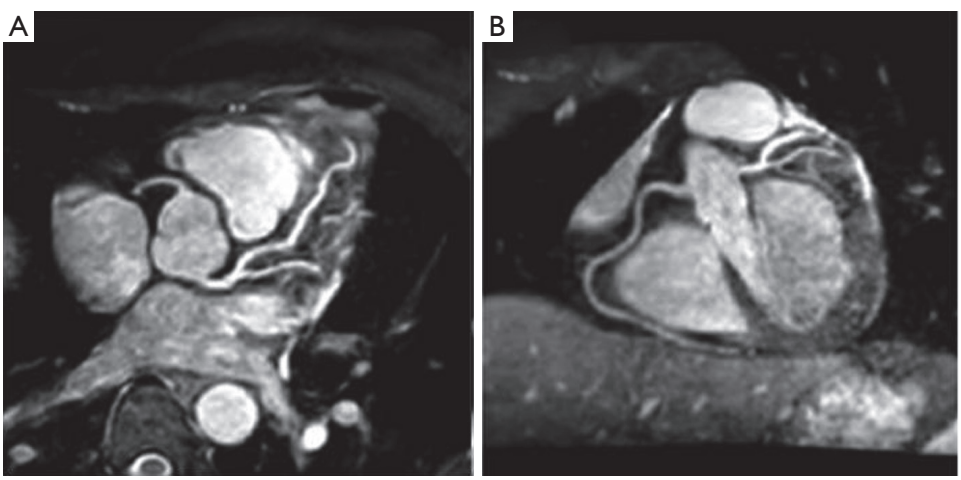

Figure 14 Representative images showing a navigator guided high spatial resolution 3D gradient-echo acquisition of the coronary arteries. A portion of the data necessary for constructing the 3D volume is acquired during each heartbeat at mid diastole, when coronary blood flow velocity is maximized. To maximize the contrast between the flowing blood and the surrounding, both muscle suppression (T_2-preparation) and fat suppression pulses are applied to suppress signal from tissue surrounding the coronary arteries.

as a fat suppression pulse are applied to suppress signal from tissue surrounding the coronary arteries (*Figure 14*).

The main drawback of navigator guided, coronary artery imaging techniques is that they are time consuming, and at present are limited to visualizing only the proximal to mid portions of the coronary artery system, and to rule out the presence of anomalous coronary arteries. This is an active area of research.

Looking forward

Recent methodological and technological advances in MR have made it possible to generate parameteric MR images of tissue T_1, T_2, and T_2*. These parametric maps yield objective measures to characterize clinical conditions such as iron overload (T_2*), fatty/fibrous infiltration (T_1), and myocardial edema in the context of myocardial infarction (T_2). From a methodological point of view, some of the major speed related limitations of CMR are currently being addressed with the incorporation of faster imaging techniques such as k-t SENSE and k-t PCA based reconstructions into routine clinical practice. The clinical availability of MR contrast agents such as Manganese ions can fundamentally alter the role of MR perfusion imaging in clinical practice.

In conclusion, CMR provides a number of key tools to the clinician to evaluate cardiovascular pathologies. Among available imaging modalities to assess global and regional ventricular function, cine cardiac MR based measurements are considered the 'gold standard'. While more involved than echo-ultrasound, CMR based phase contrast methods are robust in the evaluation of regurgitant volume, and valvular function. CMR measurement of myocardial viability using DE-MRI has been shown to be accurate, reproducible, and provides valuable prognostic information. Several studies have demonstrated that CMR stress perfusion provides at least as comparable diagnostic information as SPECT without the associated radiation burden. Lastly, ongoing developments in enhancing the tissue characterization abilities of MR may make it possible to evaluate non-ischemic cardiomyopathies such as sarcoidosis (93,94), iron overload (95-98), and fatty infiltration (99-102) on routine clinical scanners.

Acknowledgements

The authors are grateful to Ms. Feifei Qu for her valuable editorial assistance in the preparation of this manuscript.

Dr. Raja Muthupillai receives research support from Philips Health care.

Disclosure: The authors declare no conflict of interest.

References

1. Hendel RC, Patel MR, Kramer CM, et al. ACCF/ACR/SCCT/SCMR/ASNC/NASCI/SCAI/SIR 2006 appropriateness criteria for cardiac computed tomography and cardiac magnetic resonance imaging: a report of the American College of Cardiology Foundation Quality Strategic Directions Committee Appropriateness Criteria Working Group, American College of Radiology, Society of Cardiovascular Computed Tomography, Society for Cardiovascular Magnetic Resonance, American Society of Nuclear Cardiology, North American Society for Cardiac Imaging, Society for Cardiovascular Angiography and Interventions, and Society of Interventional Radiology. J Am Coll Cardiol 2006;48:1475-97.
2. Ridgway JP. Cardiovascular magnetic resonance physics for clinicians: part I. J Cardiovasc Magn Reson 2010;12:71.
3. Biglands JD, Radjenovic A, Ridgway JP. Cardiovascular magnetic resonance physics for clinicians: Part II. J Cardiovasc Magn Reson 2012;14:66.
4. Kim RJ, Chen EL, Lima JA, et al. Myocardial Gd-DTPA kinetics determine MRI contrast enhancement and reflect the extent and severity of myocardial injury after acute reperfused infarction. Circulation 1996;94:3318-26.
5. Kim RJ, Fieno DS, Parrish TB, et al. Relationship of MRI delayed contrast enhancement to irreversible injury, infarct age, and contractile function. Circulation 1999;100:1992-2002.
6. Kim RJ, Wu E, Rafael A, et al. The use of contrast-enhanced magnetic resonance imaging to identify reversible myocardial dysfunction. N Engl J Med 2000;343:1445-53.
7. Sekihara K. Steady-state magnetizations in rapid NMR imaging using small flip angles and short repetition intervals. IEEE Trans Med Imaging 1987;6:157-64.
8. Christiansen JP, Karamitsos TD, Myerson SG, et al. Stress perfusion imaging using cardiovascular magnetic resonance: a review. Heart Lung Circ 2010;19:697-705.
9. Nunnally RL, Babcock EE, Horner SD, et al. Fluorine-19 NMR spectroscopy and imaging investigations of myocardial perfusion and cardiac function. Magn Reson Imaging 1985;3:399-405.
10. Beer M, Sandstede J, Weilbach F, et al. Cardiac metabolism and function in patients with multiple

sclerosis: a combined 31P-MR-spectroscopy and MRI study. Rofo 2001;173:399-404.
11. Bruder O, Wagner A, Lombardi M, et al. European Cardiovascular Magnetic Resonance (EuroCMR) registry--multi national results from 57 centers in 15 countries. J Cardiovasc Magn Reson 2013;15:9.
12. Haacke EM, Brown RW, Thompson MR, et al. eds. Magnetic Resonance Imaging-Physical Principles and Sequence Design. Wiley-Liss, 1999.
13. Wang Y, Riederer SJ, Ehman RL. Respiratory motion of the heart: kinematics and the implications for the spatial resolution in coronary imaging. Magn Reson Med 1995;33:713-9.
14. Lenz GW, Haacke EM, White RD. Retrospective cardiac gating: a review of technical aspects and future directions. Magn Reson Imaging 1989;7:445-55.
15. Wang Y, Vidan E, Bergman GW. Cardiac motion of coronary arteries: variability in the rest period and implications for coronary MR angiography. Radiology 1999;213:751-8.
16. Ehman RL, McNamara MT, Pallack M, et al. Magnetic resonance imaging with respiratory gating: techniques and advantages. AJR Am J Roentgenol 1984;143:1175-82.
17. Bailes DR, Gilderdale DJ, Bydder GM, et al. Respiratory ordered phase encoding (ROPE): a method for reducing respiratory motion artefacts in MR imaging. J Comput Assist Tomogr 1985;9:835-8.
18. Korin HW, Farzaneh F, Wright RC, et al. Compensation for effects of linear motion in MR imaging. Magn Reson Med 1989;12:99-113.
19. Ehman RL, Felmlee JP. Adaptive technique for high-definition MR imaging of moving structures. Radiology 1989;173:255-63.
20. Botnar RM, Stuber M, Danias PG, et al. Coronary magnetic resonance angiography. Cardiol Rev 2001;9:77-87.
21. Spuentrup E, Stuber M, Botnar RM, et al. The impact of navigator timing parameters and navigator spatial resolution on 3D coronary magnetic resonance angiography. J Magn Reson Imaging 2001;14:311-8.
22. Stuber M, Botnar RM, Danias PG, et al. Double-oblique free-breathing high resolution three-dimensional coronary magnetic resonance angiography. J Am Coll Cardiol 1999;34:524-31.
23. Haacke EM, Lenz GW. Improving MR image quality in the presence of motion by using rephasing gradients. AJR Am J Roentgenol 1987;148:1251-8.
24. Axel L, Morton D. MR flow imaging by velocity-compensated/uncompensated difference images. J Comput Assist Tomogr 1987;11:31-4.
25. Ehman RL, Felmlee JP. Flow artifact reduction in MRI: a review of the roles of gradient moment nulling and spatial presaturation. Magn Reson Med 1990;14:293-307.
26. Schülen V, Schick F, Loichat J, et al. Evaluation of K-space segmented cine sequences for fast functional cardiac imaging. Invest Radiol 1996;31:512-22.
27. van der Meulen P, Groen JP, Tinus AM, et al. Fast Field Echo imaging: an overview and contrast calculations. Magn Reson Imaging 1988;6:355-68.
28. Edelman RR, Wielopolski P, Schmitt F. Echo-planar MR imaging. Radiology 1994;192:600-12.
29. Wielopolski PA, Manning WJ, Edelman RR. Single breath-hold volumetric imaging of the heart using magnetization-prepared 3-dimensional segmented echo planar imaging. J Magn Reson Imaging 1995;5:403-9.
30. Kilner PJ, Firmin DN, Rees RS, et al. Valve and great vessel stenosis: assessment with MR jet velocity mapping. Radiology 1991;178:229-35.
31. van der Meulen P, Groen JP, Cuppen JJ. Very fast MR imaging by field echoes and small angle excitation. Magn Reson Imaging 1985;3:297-9.
32. Thiele H, Nagel E, Paetsch I, et al. Functional cardiac MR imaging with steady-state free precession (SSFP) significantly improves endocardial border delineation without contrast agents. J Magn Reson Imaging 2001;14:362-7.
33. Thiele H, Paetsch I, Schnackenburg B, et al. Improved accuracy of quantitative assessment of left ventricular volume and ejection fraction by geometric models with steady-state free precession. J Cardiovasc Magn Reson 2002;4:327-39.
34. Alfakih K, Thiele H, Plein S, et al. Comparison of right ventricular volume measurement between segmented k-space gradient-echo and steady-state free precession magnetic resonance imaging. J Magn Reson Imaging 2002;16:253-8.
35. Sechtem U, Pflugfelder PW, Gould RG, et al. Measurement of right and left ventricular volumes in healthy individuals with cine MR imaging. Radiology 1987;163:697-702.
36. Longmore DB, Klipstein RH, Underwood SR, et al. Dimensional accuracy of magnetic resonance in studies of the heart. Lancet 1985;1:1360-2.
37. Park JH, Han MC, Im JG, et al. Mitral stenosis: evaluation with MR imaging after percutaneous balloon valvuloplasty. Radiology 1990;177:533-6.
38. Kondo C, Caputo GR, Semelka R, et al. Right and left

ventricular stroke volume measurements with velocity-encoded cine MR imaging: in vitro and in vivo validation. AJR Am J Roentgenol 1991;157:9-16.
39. Semelka RC, Tomei E, Wagner S, et al. Interstudy reproducibility of dimensional and functional measurements between cine magnetic resonance studies in the morphologically abnormal left ventricle. Am Heart J 1990;119:1367-73.
40. Van Rossum AC, Visser FC, Sprenger M, et al. Evaluation of magnetic resonance imaging for determination of left ventricular ejection fraction and comparison with angiography. Am J Cardiol 1988;62:628-33.
41. van Rossum AC, Visser FC, van Eenige MJ, et al. Magnetic resonance imaging of the heart for determination of ejection fraction. Int J Cardiol 1988;18:53-63.
42. Semelka RC, Tomei E, Wagner S, et al. Normal left ventricular dimensions and function: interstudy reproducibility of measurements with cine MR imaging. Radiology 1990;174:763-8.
43. Myerson SG, Montgomery HE, Whittingham M, et al. Left ventricular hypertrophy with exercise and ACE gene insertion/deletion polymorphism: a randomized controlled trial with losartan. Circulation 2001;103:226-30.
44. Bellenger NG, Davies LC, Francis JM, et al. Reduction in sample size for studies of remodeling in heart failure by the use of cardiovascular magnetic resonance. J Cardiovasc Magn Reson 2000;2:271-8.
45. Simonetti OP, Finn JP, White RD, et al. "Black blood" T2-weighted inversion-recovery MR imaging of the heart. Radiology 1996;199:49-57.
46. Fleckenstein JL, Archer BT, Barker BA, et al. Fast short-tau inversion-recovery MR imaging. Radiology 1991;179:499-504.
47. McMahon CJ, Su JT, Taylor MD, et al. Images in cardiovascular medicine. Detection of active coronary arterial vasculitis using magnetic resonance imaging in Kawasaki disease. Circulation 2005;112:e315-6.
48. Yarnykh VL, Yuan C. T1-insensitive flow suppression using quadruple inversion-recovery. Magn Reson Med 2002;48:899-905.
49. Yarnykh VL, Yuan C. Simultaneous outer volume and blood suppression by quadruple inversion-recovery. Magn Reson Med 2006;55:1083-92.
50. Stuber M, Botnar RM, Spuentrup E, et al. Three-dimensional high-resolution fast spin-echo coronary magnetic resonance angiography. Magn Reson Med 2001;45:206-11.
51. Wince WB, Kim RJ. Molecular imaging: T2-weighted CMR of the area at risk--a risky business? Nat Rev Cardiol 2010;7:547-9.
52. Aletras AH, Kellman P, Derbyshire JA, et al. ACUT2E TSE-SSFP: a hybrid method for T2-weighted imaging of edema in the heart. Magn Reson Med 2008;59:229-35.
53. Kellman P, Aletras AH, Mancini C, et al. T2-prepared SSFP improves diagnostic confidence in edema imaging in acute myocardial infarction compared to turbo spin echo. Magn Reson Med 2007;57:891-7.
54. Giri S, Chung YC, Merchant A, et al. T2 quantification for improved detection of myocardial edema. J Cardiovasc Magn Reson 2009;11:56.
55. Dinsmore RE, Wismer GL, Miller SW, et al. Magnetic resonance imaging of the heart using image planes oriented to cardiac axes: experience with 100 cases. AJR Am J Roentgenol 1985;145:1177-83.
56. Akins EW, Hill JA, Sievers KW, et al. Assessment of left ventricular wall thickness in healed myocardial infarction by magnetic resonance imaging. Am J Cardiol 1987;59:24-8.
57. White RD, Cassidy MM, Cheitlin MD, et al. Segmental evaluation of left ventricular wall motion after myocardial infarction: magnetic resonance imaging versus echocardiography. Am Heart J 1988;115:166-75.
58. Moran PR. A flow velocity zeugmatographic interlace for NMR imaging in humans. Magn Reson Imaging 1982;1:197-203.
59. Pelc NJ, Bernstein MA, Shimakawa A, et al. Encoding strategies for three-direction phase-contrast MR imaging of flow. J Magn Reson Imaging 1991;1:405-13.
60. Conturo TE, Robinson BH. Analysis of encoding efficiency in MR imaging of velocity magnitude and direction. Magn Reson Med 1992;25:233-47.
61. Yoganathan AP, Cape EG, Sung HW, et al. Review of hydrodynamic principles for the cardiologist: applications to the study of blood flow and jets by imaging techniques. J Am Coll Cardiol 1988;12:1344-53.
62. Chatzimavroudis GP, Walker PG, Oshinski JN, et al. The importance of slice location on the accuracy of aortic regurgitation measurements with magnetic resonance phase velocity mapping. Ann Biomed Eng 1997;25:644-52.
63. Chatzimavroudis GP, Walker PG, Oshinski JN, et al. Slice location dependence of aortic regurgitation measurements with MR phase velocity mapping. Magn Reson Med 1997;37:545-51.
64. Hamilton CA. Correction of partial volume inaccuracies in quantitative phase contrast MR angiography. Magn Reson Imaging 1994;12:1127-30.

65. Tang C, McVeigh ER, Zerhouni EA. Multi-shot EPI for improvement of myocardial tag contrast: comparison with segmented SPGR. Magn Reson Med 1995;33:443-7.
66. Tang C, Blatter DD, Parker DL. Correction of partial-volume effects in phase-contrast flow measurements. J Magn Reson Imaging 1995;5:175-80.
67. Hoogeveen RM, Bakker CJ, Viergever MA. MR phase-contrast flow measurement with limited spatial resolution in small vessels: value of model-based image analysis. Magn Reson Med 1999;41:520-8.
68. Nesto RW, Kowalchuk GJ. The ischemic cascade: temporal sequence of hemodynamic, electrocardiographic and symptomatic expressions of ischemia. Am J Cardiol 1987;59:23C-30C.
69. Al Jaroudi W, Iskandrian AE. Regadenoson: a new myocardial stress agent. J Am Coll Cardiol 2009;54:1123-30.
70. Donahue KM, Weisskoff RM, Burstein D. Water diffusion and exchange as they influence contrast enhancement. J Magn Reson Imaging 1997;7:102-10.
71. Nagel E, Klein C, Paetsch I, et al. Magnetic resonance perfusion measurements for the noninvasive detection of coronary artery disease. Circulation 2003;108:432-7.
72. Klocke FJ, Simonetti OP, Judd RM, et al. Limits of detection of regional differences in vasodilated flow in viable myocardium by first-pass magnetic resonance perfusion imaging. Circulation 2001;104:2412-6.
73. Sourbron S. Technical aspects of MR perfusion. Eur J Radiol 2010;76:304-13.
74. Kim HW, Lee D, Pohost GM. (31)P cardiovascular magnetic resonance spectroscopy: a unique approach to the assessment of the myocardium. Future Cardiol 2009;5:523-7.
75. Jerosch-Herold M, Muehling O. Stress perfusion magnetic resonance imaging of the heart. Top Magn Reson Imaging 2008;19:33-42.
76. Jerosch-Herold M, Seethamraju RT, Swingen CM, et al. Analysis of myocardial perfusion MRI. J Magn Reson Imaging 2004;19:758-70.
77. Schwitter J. Myocardial perfusion imaging by cardiac magnetic resonance. J Nucl Cardiol 2006;13:841-54.
78. Wang Y, Moin K, Akinboboye O, et al. Myocardial first pass perfusion: steady-state free precession versus spoiled gradient echo and segmented echo planar imaging. Magn Reson Med 2005;54:1123-9.
79. Cheng AS, Pegg TJ, Karamitsos TD, et al. Cardiovascular magnetic resonance perfusion imaging at 3-tesla for the detection of coronary artery disease: a comparison with 1.5-tesla. J Am Coll Cardiol 2007;49:2440-9.
80. Manka R, Vitanis V, Boesiger P, et al. Clinical feasibility of accelerated, high spatial resolution myocardial perfusion imaging. JACC Cardiovasc Imaging 2010;3:710-7.
81. Motwani M, Maredia N, Fairbairn TA, et al. High-resolution versus standard-resolution cardiovascular MR myocardial perfusion imaging for the detection of coronary artery disease. Circ Cardiovasc Imaging 2012;5:306-13.
82. Schwitter J, Wacker CM, Wilke N, et al. MR-IMPACT II: Magnetic Resonance Imaging for Myocardial Perfusion Assessment in Coronary artery disease Trial: perfusion-cardiac magnetic resonance vs. single-photon emission computed tomography for the detection of coronary artery disease: a comparative multicentre, multivendor trial. Eur Heart J 2013;34:775-81.
83. Greenwood JP, Maredia N, Younger JF, et al. Cardiovascular magnetic resonance and single-photon emission computed tomography for diagnosis of coronary heart disease (CE-MARC): a prospective trial. Lancet 2012;379:453-60.
84. Rahimtoola SH, Dilsizian V, Kramer CM, et al. Chronic ischemic left ventricular dysfunction: from pathophysiology to imaging and its integration into clinical practice. JACC Cardiovasc Imaging 2008;1:536-55.
85. Hamon M, Fau G, Nee G, et al. Meta-analysis of the diagnostic performance of stress perfusion cardiovascular magnetic resonance for detection of coronary artery disease. J Cardiovasc Magn Reson 2010;12:29.
86. Schvartzman PR, Srichai MB, Grimm RA, et al. Nonstress delayed-enhancement magnetic resonance imaging of the myocardium predicts improvement of function after revascularization for chronic ischemic heart disease with left ventricular dysfunction. Am Heart J 2003;146:535-41.
87. Selvanayagam JB, Kardos A, Francis JM, et al. Value of delayed-enhancement cardiovascular magnetic resonance imaging in predicting myocardial viability after surgical revascularization. Circulation 2004;110:1535-41.
88. Schinkel AF, Poldermans D, Rizzello V, et al. Why do patients with ischemic cardiomyopathy and a substantial amount of viable myocardium not always recover in function after revascularization? J Thorac Cardiovasc Surg 2004;127:385-90.
89. Schinkel AF, Bax JJ, Poldermans D, et al. Hibernating myocardium: diagnosis and patient outcomes. Curr Probl Cardiol 2007;32:375-410.
90. Rizzello V, Schinkel AF, Bax JJ, et al. Individual prediction of functional recovery after coronary revascularization in patients with ischemic cardiomyopathy: the scar-to-

biphasic model. Am J Cardiol 2003;91:1406-9.
91. Glaveckaite S, Valeviciene N, Palionis D, et al. Value of scar imaging and inotropic reserve combination for the prediction of segmental and global left ventricular functional recovery after revascularisation. J Cardiovasc Magn Reson 2011;13:35.
92. Wellnhofer E, Olariu A, Klein C, et al. Magnetic resonance low-dose dobutamine test is superior to SCAR quantification for the prediction of functional recovery. Circulation 2004;109:2172-4.
93. Cheong BY, Muthupillai R, Nemeth M, et al. The utility of delayed-enhancement magnetic resonance imaging for identifying nonischemic myocardial fibrosis in asymptomatic patients with biopsy-proven systemic sarcoidosis. Sarcoidosis Vasc Diffuse Lung Dis 2009;26:39-46.
94. Khan R, Tweedie EJ, Pflugfelder PW, et al. Cardiac sarcoid in a heart transplant recipient: detection with cardiac magnetic resonance imaging. Transplant Proc 2010;42:1976-8.
95. Anderson LJ. Assessment of iron overload with T2* magnetic resonance imaging. Prog Cardiovasc Dis 2011;54:287-94.
96. Anderson LJ, Holden S, Davis B, et al. Cardiovascular T2-star (T2*) magnetic resonance for the early diagnosis of myocardial iron overload. Eur Heart J 2001;22:2171-9.
97. Anderson LJ, Westwood MA, Holden S, et al. Myocardial iron clearance during reversal of siderotic cardiomyopathy with intravenous desferrioxamine: a prospective study using T2* cardiovascular magnetic resonance. Br J Haematol 2004;127:348-55.
98. Carpenter JP, He T, Kirk P, et al. On T2* magnetic resonance and cardiac iron. Circulation 2011;123:1519-28.
99. Abbara S, Migrino RQ, Sosnovik DE, et al. Value of fat suppression in the MRI evaluation of suspected arrhythmogenic right ventricular dysplasia. AJR Am J Roentgenol 2004;182:587-91.
100. Castillo E, Tandri H, Rodriguez ER, et al. Arrhythmogenic right ventricular dysplasia: ex vivo and in vivo fat detection with black-blood MR imaging. Radiology 2004;232:38-48.
101. Jacquier A, Bressollette E, Laissy JP, et al. MR imaging and arrhythmogenic right ventricular dysplasia (ARVD). J Radiol 2004;85:721-4.
102. Wu YW, Tadamura E, Kanao S, et al. Structural and functional assessment of arrhythmogenic right ventricular dysplasia/cardiomyopathy by multi-slice computed tomography: comparison with cardiovascular magnetic resonance. Int J Cardiol 2007;115:e118-21.

Cite this article as: Krishnamurthy R, Cheong B, Muthupillai R. Tools for cardiovascular magnetic resonance imaging. Cardiovasc Diagn Ther 2014;4(2):104-125. doi: 10.3978/j.issn.2223-3652.2014.03.06

